Scripta Materialia 118 (2016) 51–54

Contents lists available at ScienceDirect

Scripta Materialia

journal homepage: www.elsevier.com/locate/scriptamat

Ultrahigh tensile transformation strains in new $Ni_{50.5}Ti_{36.2}Hf_{13.3}$ shape memory alloy

Y. Wu [a], L. Patriarca [a], H. Sehitoglu [a,*], Y. Chumlyakov [b]

[a] Department of Mechanical Science and Engineering, University of Illinois at Urbana–Champaign, 1206 W. Green St., Urbana, IL 61801, USA
[b] Siberian Physical–Technical Institute at Tomsk State University, Tomsk 634050, Russia

ARTICLE INFO

Article history:
Received 21 November 2015
Received in revised form 8 February 2016
Accepted 8 March 2016
Available online xxxx

Keywords:
NiTiHf
Single crystals
Shape memory effect
Superelasticity
Digital image correlation

ABSTRACT

We report on unprecedented transformation strains exceeding 20% in tension for $Ni_{50.5}Ti_{36.2}Hf_{13.3}$ shape memory alloy (SMA). The strain measurements were made at multiscales utilizing advanced digital image correlation. The display of excellent strain reversibility in shape memory (isothermal deformation between M_f and A_f), isobaric thermal cycling (between M_f and A_f), and superelasticity experiments (deformation above A_f) confirms a wide range of functionality. The ultrahigh strains in [111] orientation exceed the lattice deformation theory predictions possibly pointing to contributions from mechanical twinning effects. The high strength levels and large strains result in very high work outputs compared to other SMAs.

1. Introduction

Research on SMAs has considerable merit as these materials are increasingly used in various technological applications [1–3]. The binary NiTi represents the most widely studied SMA material with transformation strains reaching 10% in tension [4–6]. Recently, considerable efforts have been made to seek ternary additions for extra functionality such as control of transformation temperatures and hysteresis [7–9]. The addition of ternary elements can produce lower transformation strain levels and lower slip strength in many cases compared to binary NiTi [10]. One of the most well-known ternary additions is Cu which results in transformation strains and plastic slip resistance below NiTi [11] (see Figure 6 in [12] for example). Other ternary additions [7] also decrease the transformation strains and in many cases lower the slip resistance. It is imperative to seek enhancements in dislocation slip resistance to improve long-term durability and increase in transformation strains to expand the SMA's functionality. The ternary addition of hafnium (Hf) can enhance the critical stress for slip [13], and also the theoretical transformation strains [6,12].

The single crystals are the best choice for studying the transformation strains as they circumvent the grain boundary effects. Based on our calculations, the single crystals of NiTiHf ternary alloys are expected to demonstrate high transformation strain levels (>14%) in tension. However, experiments in tension demonstrating such high strains are still lacking. In this work, the shape memory and superelastic strains are reported in [111] oriented $Ni_{50.5}Ti_{36.2}Hf_{13.3}$ (at.%) (referred to as NiTi–13.3Hf in the paper) single crystal. Three types of experiments were conducted for a complete characterization. In the first case, the specimens displayed shape memory behavior and recovery were achieved upon heating at zero stress. In the second case, the experiments were conducted in the superelastic regime where the strain recovery was observed upon unloading. In the third case, thermal cycling was performed under constant stress. All three cases corresponded to high strains (surprisingly as high as 21.5%) confirming a wide range of functionality.

The strain measurements were made using digital image correlation (DIC) techniques at high magnifications developed in our laboratory [14,15] and represent an improvement over previous techniques as discussed below. Previous research [16–19] was carried out using traditional extensometry through averaging strains over a large volume which contains both transformed (M) and untransformed domains (A). A high resolution DIC is needed for precise measurements of transformation strain at small scales. Therefore, the intrinsic transformation strains were investigated by using a [111] single crystal selected for highest transformation strains. In this work, we demonstrate that ultrahigh transformation strain can be obtained in a NiTi–13.3Hf single crystal.

The measured strains are compared with the theoretical values obtained via lattice deformation theory. Because the theoretical transformation strains are very sensitive to the choice of lattice constants, the lattice constants were carefully determined via X-ray diffraction patterns in austenite and confirmed with DFT (Density Functional Theory, VASP [20]) calculations. In the case of martensite, the lattice parameters were determined based on DFT calculations [13].

* Corresponding author.
E-mail address: huseyin@illinois.edu (H. Sehitoglu).

http://dx.doi.org/10.1016/j.scriptamat.2016.03.009
1359-6462/

In summary, with high strains exceeding 20%, the NiTi–13.3Hf ternary alloy presents extraordinary promise. Combined with its high slip resistance exceeding a critical resolved shear stress (CRSS) of 430 MPa based on theory [13] and 424 MPa based on experiments in this study, it holds great potential as a SMA. Thus, the utilization of this class of materials in engineering applications can occur where high transformation strains and high strength are desired. The methodologies (ranging from atomistic calculations to X-Ray diffraction, lattice constant and slip stress determination and local strain measurement in single crystals utilizing advanced DIC) can be applied effectively for better understanding of NiTiHf class of alloys.

2. Experimental methods

The polycrystalline alloys with a nominal composition of $Ni_{50.5}Ti_{36.2}Hf_{13.3}$ (at.%) were produced by plasma arc melting. Subsequently, single crystals were grown utilizing the Bridgman technique in He atmosphere. The chemical compositions of the single crystal were checked with ICP-MS instrument. Thin foils, 30–40 mg, were cut using a low speed diamond saw. These foils were used to measure the transformation temperatures of the alloy in the as-grown condition with a Perkin–Elmer Pyris 1 differential scanning calorimetry (DSC) machine.

Prior to any experiments, tension samples were carefully sectioned from the single crystal ingot with a dimension of 2 mm × 2 mm × 8 mm in the gauge section using an electrical discharge machine with the loading direction along the $[111]_{B2}$ crystallographic orientation. The sample surface was polished to a mirror finish with abrasive papers up to 1800 grit. A fine speckle pattern was airbrushed on the surface for DIC strain measurements. A Lepel induction generator was used to control the operating temperature on the specimen. The sample was initially heated above A_f (austenite finish temperature) to stabilize the speckle pattern and successively slowly cooled to the desired temperature. In order to test the sample at subzero conditions, the grips were cooled using liquid nitrogen through customized copper coils. Then, the sample was tested in tension at various temperatures with an Instron servo hydraulic load frame. The load frame was controlled by a customized LabView software during loading and unloading with the capability of taking images automatically. A reference image at zero load was taken with an image resolution of 2.0 μm/pixel. The images captured during the loading and unloading cycle were captured every 2 s. The DIC strain fields were determined using a commercial software VIC-2D by correlating the reference images with the deformed images.

X-ray diffraction and crystal orientation analysis were conducted on a Philips Xpert 2 diffractometer using Cu Kα radiation at room temperature. A Ni filter was used to suppress the K_β wavelength [21]. The voltage and current are set to be 45 kV and 40 mA respectively.

3. Experimental results

The transformation temperatures for NiTi–13.3Hf single crystal in the as-grown condition were determined by using DSC. For the as-grown condition, M_s (martensite start temperature) was measured as −31.7 °C, M_f (martensite finish temperature) = −69.4 °C, A_s (austenite start temperature) = −14.8 °C, and A_f = 31.2 °C.

The X-ray diffraction was used to determine the [111] crystal orientation of the NiTi–13.3Hf tensile specimen. The experimental inverse pole figures constructed from the X-ray data are presented in Fig. 1. The results show that along the loading direction the specimen is properly oriented along the [111] orientation, while the normal to the specimen plane is parallel to the [011] crystal direction. The X-ray diffraction pattern is also reported in Fig. 1. Peaks of the cubic (B2) austenite appear following the reflection of the $\{011\}_{B2}$ and $\{022\}_{B2}$ planes. The lattice constant of the cubic B2 austenite was calculated from the position of the {011} and {022} peaks to be a_o = 3.0641 A.

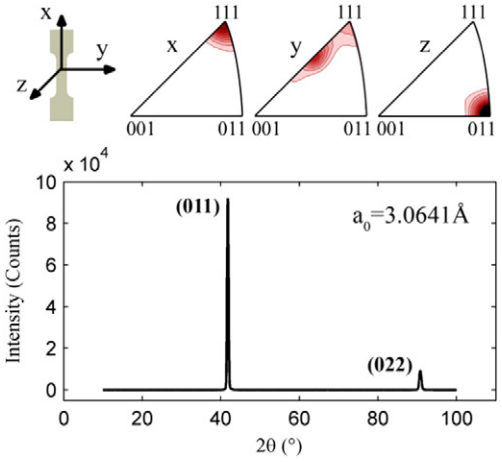

Fig. 1. X-ray diffraction pattern and inverse pole figure obtained on NiTi–13.3Hf showing the microstructure and specimen orientation.

For the monoclinic martensite (B19′) structure, the lattice parameters were obtained for several compositions utilizing DFT [13] and then interpolated to obtain the following values: a = 2.986 Å, b = 4.0728 Å, c = 4.786 Å, γ = 99.9°.

The details of the calculation procedures utilizing LDT are explained in [22], so it is not covered for the sake of brevity. In Fig. 2, the stereographic triangle exhibiting transformation strain contours from LDT are presented. The highest strains are near the <111> pole where the maximum transformation strain was as high as 14.2%.

In Fig. 3a, we report the isothermal behavior in tension. The black curve demonstrates the stress–strain behavior over a wide domain (2 mm × 4 mm) while the blue dashed line represents the local behavior (0.3 mm × 0.6 mm). The transformation stresses were 592 MPa and 850 MPa at 0 °C and 50 °C respectively. We note the downward slope of stress–strain curves in all cases. In the case of 0 °C, multiple transformation bands nucleate at 592 MPa followed by coalescence (Point B). When the maximum local strain reaches 23% (Point C), the transformation zone has widened, yet substantial elastic domains remain outside this zone. Removing the inherent elastic strains, the strain recovery is marked on the figures. In summary, $\varepsilon_{trans}^{loc}$, was as high as 21.5%, while over large domains the transformation strain, $\varepsilon_{trans}^{overall}$, was on the order of 12.7%.

A clear superelastic response was evident at 50 °C in Fig. 3a. The transformation stress is approximately 850 MPa (a corresponding CRSS, with a Schmid factor of 0.4, of 340 MPa). The maximum local strain reached was as high as 20%. Upon unloading, the majority portion of the localized strain is recovered. However, 1.5% of residual strain does not recover even after heating. At a smaller domain, the reversible strain was 18.7%. The recoverability is reduced by 2.8% compared to values at

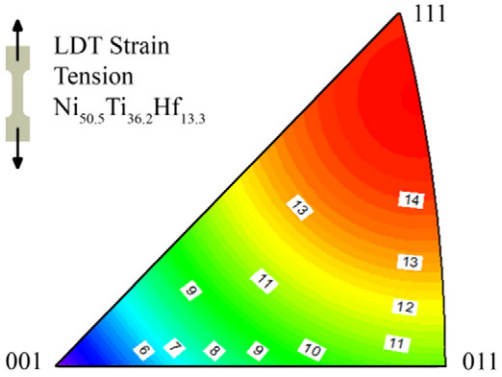

Fig. 2. Stereographic Triangle demonstrating the transformation strains in tension for NiTi–13.3Hf calculated by lattice deformation theory (LDT).

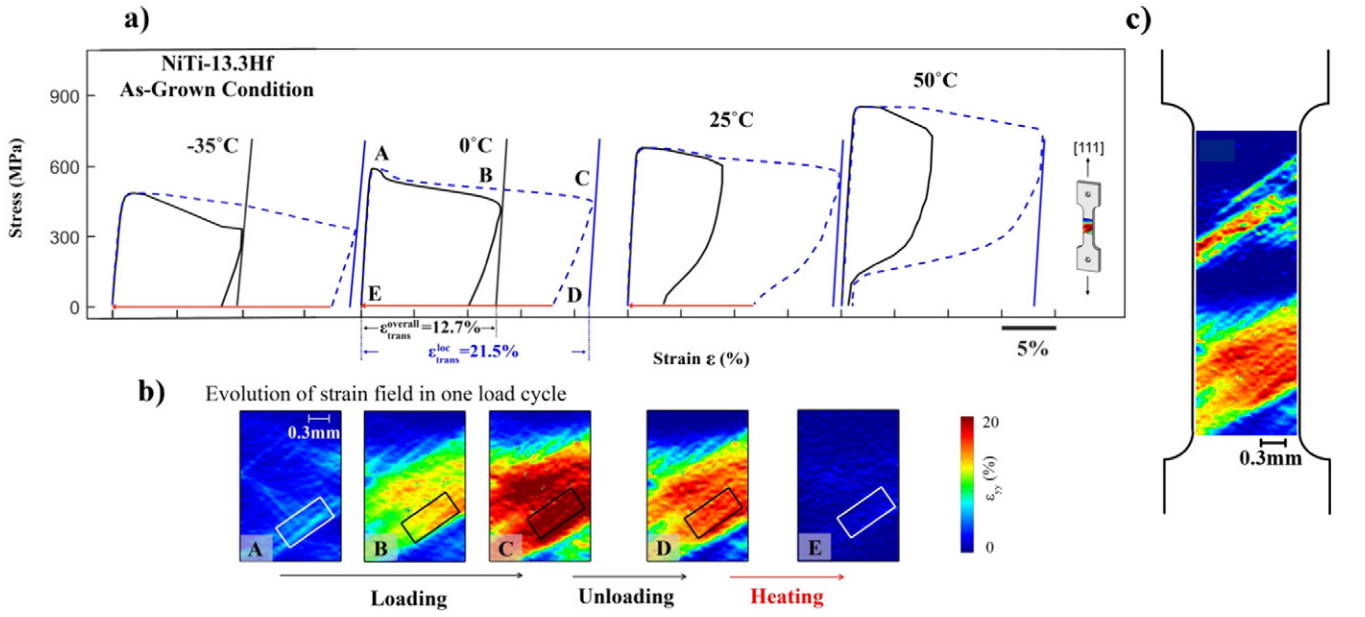

Fig. 3. a) The experimental stress–strain curves at various temperatures demonstrating the shape memory effect and superelasticity of NiTi–13.3Hf in tension in [111] direction. The overall strain is plotted in the solid black line, while the local one in the blue dashed line. The solid red arrow indicates the recoverability of strain after heating above A_f. b) The DIC strain contours are shown to demonstrate the evolution of transformation strain at different steps in one load cycle. The rectangular box displayed in the DIC images indicates the origin of local strain in part a). The maximum local and overall transformation strains, $\varepsilon^{loc}_{trans}$ and $\varepsilon^{overall}_{trans}$, are indicated on the figure. c) Strain field of the entire gauge section (2 mm × 8 mm) of the specimen at point D is presented showing the heterogeneity of the transformation.

0 °C and RT due to the higher propensity of slip deformation with higher levels of stress. The flow stress obeys a Clausius–Clapeyron type relationship with a slope of 5.6 MPa/°C.

Fig. 4 illustrates the isobaric behavior of NiTi–13.3Hf when it was temperature cycled between −50 °C to 55 °C under a tensile stress of 500 MPa. The local and overall transformation strains are 17.5% and 11.8% respectively. These measurements are close to those achieved in the isothermal experiments. Note that the transformation temperatures were increased under stress. When a 500 MPa external stress is applied,

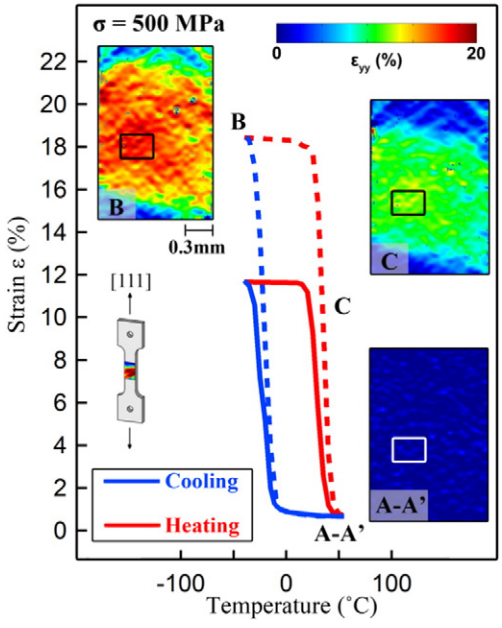

Fig. 4. Strain as a function of temperature for NiTi–13.3Hf orientated in [111] direction. The dashed line indicates the local response while the solid line overall behavior. The local strain is extracted from the rectangular area enclosed in the DIC strain contour.

M_f, M_s, A_s, and A_f under stress were −30 °C, −10 °C, 25 °C, and 45 °C, an increase of 15 °C compared to DSC results.

4. Discussion of results

The NiTi alloy is viewed as the most successful SMA to date and has attracted widespread attention. The maximum transformation strain of NiTi in [111] direction is 10% (in tension) [5,6,16]. There are several SMAs such as Ni_2FeGa that possess higher transformation strains in tension of the order of 12.5% [15]; in this study, we show that the NiTi–13.3Hf exhibits even higher strains. We demonstrate that tensile transformation strain in smaller domains (0.3 to 1 mm^3) and larger volumes (>1 mm^3) can reach 21.5% and 12.5% respectively in NiTi–13.3Hf. Including elasticity, a local maximum strain near 23% was attained without fracture which is significantly higher than ductility of most SMAs. The higher transformation strain in NiTi–13.3Hf compared to NiTi is largely attributed to the increase in the monoclinic angle, from 96.7° to 99.9°. Since the experimental strains exceed the calculated ones based on lattice constants (cubic to monoclinic transformation) and the monoclinic angle, we suggest possible contribution from mechanical twinning on the measured strains.

Most importantly, the addition of Hf to NiTi elevates the CRSS. The increase in slip resistance has been studied earlier by Wang and Sehitoglu [13] upon determination of the energy barriers (generalized stacking fault energy via DFT) for dislocation motion. The CRSS was predicted to be approximately 433 MPa which matches with the present experimental measurement of 424 MPa in this study (using {011}<100> slip system with a Schmid factor of 0.47). The combination of high transformation strain and slip resistance, suggests that the NiTi–13.3Hf represents a potentially formidable SMA worth further exploration.

As explained above, the maximum reversible strain of 21.5% exceeds the theoretical transformation strain of 14.2% by a factor of 1.5. We offer a plausible explanation of strain measurements exceeding theory based on the activation of mechanical twinning. The martensitic phase may undergo additional mechanical twinning that can also be partially or

fully reversed and contributes to the strain reversibility. Although this is difficult to prove, such twinning can occur on the {100}<001> system as documented in our early work [12] and the corresponding magnitude of twin shear has been determined from the c/a ratio of the martensite (0.62). Such a large twinning shear, if accommodated elastically, can readily contribute to the additional reversible strains observed experimentally. A similar rationale has been proposed by one of the co-authors of this paper on martensite mechanical twinning in binary NiTi single crystal exhibiting high strains [6].

In addition, as noted in the stress–strain curves of Fig. 3a, a negative slope in stress–strain response during straining is evident upon nucleation of the martensite. Clearly, a higher stress is required to nucleate the martensite embryo, while a lower stress is needed to sustain its migration in the case of NiTi–13.3Hf. This characteristic is reminiscent of transformation behavior observed in some NiTi binary alloys [23] and twinning in bcc metals [24]. In Fig. 3b, the transformation area (red zone) in NiTi–13.3Hf is confined to a small volume. The consequence of the localization is a significant difference in measured strains at macroscale and microscale. Further aging treatments to create coherent precipitates may alter this localization behavior, and reduce the micro–macro difference.

The DIC technique was used to pinpoint the domains undergoing transformation and the local strains that are representative of the 'intrinsic' transformation strain. These measurements were made in-situ during the deformation to establish precisely the onset of phase transformation, slip nucleation, and shift in transformation temperatures in isobaric experiments. For example, in Fig. 3a, the phase transformation (at 0 °C test) starts at approximately 592 MPa and stress for slip nucleation can be observed at 50 °C. In Fig. 4, the austenite to martensite transformation is captured when the temperature reaches −10 °C under isobaric condition. Therefore, the clarity achieved by DIC allows pinpointing the critical stresses and transformation temperatures under stress precisely.

The critical stress for transformation increases with temperature. This is consistent with the Clausius–Clapeyron curve with a slope of 5.6 MPa/°C which is lower compared to the compressive case [25]. The new ternary NiTi–13.3Hf alloy has a transformation stress of 850 MPa at 50 °C and combined with a maximum transformation strain in the order of 21.5% results in a work output of approximately 170 J/cm^3. This is the highest measurement among the SMAs as well. The substantial increase of the transformation stress, transformation strain, and work output can be exploited as guidance for future NiTiHf alloy developments.

5. Conclusions

This work demonstrates the ultrahigh strain recoverability of NiTi–13.3Hf single crystals orientated in [111] direction. Three types of experiments were conducted (a) transformation followed by recovery at zero stress upon heating, (b) superelasticity where recovery occurs upon unloading and (c) isobaric temperature cycling where austenite to martensite transformation occurs in a reversible fashion. Based on the current work, the following conclusions can be drawn:

(1) For the [111] oriented NiTi–13.3Hf single crystal, intrinsic transformation strain was captured by measuring the local strains via DIC. The maximum transformation strain is in the order of 21.5%. We attribute the high strains partly to the increase in monoclinic angle with the addition of Hf. Since the measured strains exceed the lattice deformation theory calculations, we forward the possibility of reversible mechanical twinning of martensite contributing to such high strains.

(2) The NiTi–13.3Hf exhibits high slip resistance with a CRSS value of 424 MPa in agreement with theoretical calculations (430 MPa). Such a high slip resistance combined with lower transformation shear stress (340 MPa) facilitates the achievement of high transformation strains and creates 'ideal' conditions for reversible martensite formation.

(3) With the maximum transformation strain as high as 21.5% and a transformation axial stress level of 850 MPa at 50 °C, the work output well exceeds 150 J/cm^3. This is a considerable advancement compared to other SMA alloys. In summary, the capability of NiTi–13.3Hf to operate under conditions of high stress and high ductility exceeds other SMAs.

Acknowledgments

The research was supported by an NSF grant CMMI-1333884. This support is gratefully acknowledged. The authors acknowledge Dr. Mauro Sardela, Materials Research Laboratory at Illinois, for his help with X-ray Diffraction measurements. Professor Chumlyakov was funded by RSF 14-29-00012.

References

[1] H. Funakubo, Shape Memory Alloys, Gordon and Breach Science Publishers, 1987 (translated from the Japanese by J.B. Kennedy).
[2] T.W. Duerig, K. Melton, D. Stockel, C. Wayman, Butterworth–Heinemann, Engineering Aspects of Shape Memory Alloys, Reed Books Services Ltd, P. O. Box 5, Rushden, Northants, NN 10 9 YX, UK, 1990 499 (1990).
[3] H. Sehitoglu, Shape Mem. Superelastic. 1 (2015) 1–3.
[4] S. Miyazaki, S. Kimura, F. Takei, T. Miura, K. Otsuka, Y. Suzuki, Scr. Metall. 17 (1983) 1057–1062.
[5] C. Efstathiou, H. Sehitoglu, Scr. Mater. 59 (2008) 1263–1266.
[6] Y. Chumlyakov, I. Kireeva, E. Panchenko, I. Karaman, H. Maier, E. Timofeeva, J. Alloys Compd. 577 (2013) S393–S398.
[7] J. Van Humbeeck, J. Eng. Mater. Technol. 121 (1999) 98–101.
[8] K. Otsuka, X. Ren, Prog. Mater. Sci. 50 (2005) 511.
[9] C.S. Zhang, L.C. Zhao, T.W. Duerig, C.M. Wayman, Scr. Metall. Mater. 24 (1990) 1807–1812.
[10] E. Patoor, D.C. Lagoudas, P.B. Entchev, L.C. Brinson, X. Gao, Mech. Mater. 38 (2006) 391–429.
[11] H. Sehitoglu, I. Karaman, X. Zhang, A. Viswanath, Y. Chumlyakov, H.J. Maier, Acta Mater. 49 (2001) 3621–3634.
[12] Y. Wu, L. Patriarca, G. Li, H. Sehitoglu, Y. Soejima, T. Ito, M. Nishida, Shape Mem. Superelastic. 1 (2015) 387–397.
[13] J. Wang, H. Sehitoglu, Philos. Mag. 94 (2014) 2297–2317.
[14] J. Carroll, W. Abuzaid, J. Lambros, H. Sehitoglu, Rev. Sci. Instrum., 81.
[15] C. Efstathiou, H. Sehitoglu, J. Carroll, J. Lambros, H.J. Maier, Acta Mater. 56 (2008) 3791–3799.
[16] S. Miyazaki, K. Otsuka, Y. Suzuki, Scr. Metall. 15 (1981) 287–292.
[17] G. Bigelow, A. Garg, S. Padula, D. Gaydosh, R. Noebe, Scr. Mater. 64 (2011) 725–728.
[18] O. Benafan, R. Noebe, S. Padula II, R. Vaidyanathan, Metall. Mater. Trans. A 43 (2012) 4539–4552.
[19] D.R. Coughlin, P.J. Phillips, G.S. Bigelow, A. Garg, R.D. Noebe, M.J. Mills, Scr. Mater. 67 (2012) 112–115.
[20] G. Kresse, J. Furthmuller, Phys. Rev. B Condens. Matter 54 (1996) 11169.
[21] P. Potapov, A. Shelyakov, A. Gulyaev, E. Svistunov, N. Matveeva, D. Hodgson, Mater. Lett. 32 (1997) 247–250.
[22] H. Sehitoglu, I. Karaman, R. Anderson, X. Zhang, K. Gall, H. Maier, Y. Chumlyakov, Acta Mater. 48 (2000) 3311–3326.
[23] J.A. Shaw, S. Kyriakides, J. Mech. Phys. Solids 43 (1995) 1243–1281.
[24] A. Ojha, H. Sehitoglu, L. Patriarca, H. Maier, Philos. Mag. 94 (2014) 1816–1840.
[25] H.E. Karaca, S.M. Saghaian, B. Basaran, G.S. Bigelow, R.D. Noebe, Y.I. Chumlyakov, Scr. Mater. 65 (2011) 577–580.